International Journal of Analytical, Experimental and Finite Element Analysis
Volume 9, Issue 3, Sept 2022, pp 50 - 61
https://doi.org/10.26706/ijaefea.3.9.2211163

Phase Change Analysis of Robot Laser Drilling with Accuracy Enhancement by Deep Learning

Jihad Kadhim AbdAli [1,2,*] and Maysoon Khazaal Abbas Maaroof [2]

[1] Ph.D. Power Mechanical Engineering, Field Crops Dept., Agricultural College, Al.Qasim Green University, Babil, Iraq.
[2] Msc. Information Technology. Basic Education College, University of Babylon, Babil, Iraq

jihadhpvit@gmail.com Email: maysoonalmaroof@gmail.com

[*] Corresponding Author: jihadhpvit@gmail.com

Abstract: In this investigations, heat transfer mechanism of laser drilling process is analyzed by using Matlab program 8.5. Calculations of the heat impacted zone were also done. The moving boundary condition generates phase shift and influences heat transfer during the laser drilling process. The classical approach is used to study heat conduction in solids, with modifications made to account for the boundary condition transition from Stefan to continuous heat flow. According to the suggested model, for a given laser beam intensity and pulse time, the drilling hole profiles in a certain material will be quite near to one another. Robot placement errors are complicated since there are many different sources for them, programming in the python language examined. The positioning precision of the robot is improved, and its application capabilities are increased, to reinforced machine learning. The suggested methodology offers a simple and direct method for real-time robot position modification in industrial settings during production setup or readjustment situations. a deep learning approach used to increase the operational positioning precision of an articulated robot. Approximately 300 iterations later, the placement accuracy had significantly improved.

Keywords: laser drilling, phase change phenomenon, deep learning, position error

Article – Peer Reviewed
Received: 28 Sept 2022
Accepted: 11 Oct 2022
Published: 14 Oct 2022

Cite this article: Jihad Kadhim AbdAli and Maysoon Khazaal Abbas Maaroof, "Phase Change Analysis of Robot Laser Drilling with Accuracy Enhancement by Deep Learning", *International Journal of Analytical, Experimental and Finite Element Analysis*, RAME Publishers, vol. 9, issue 3, pp. 50-61, 2022. https://doi.org/10.26706/ijaefea.3.9.2211163

1. Introduction

A laser beam with a high-power density, material from the workpiece is melted or vaporized during laser drilling. In theory, the energy balance for the energy radiated by the laser beam and the heat that is transferred into the material, the energy diffusion to the surrounding, and the energy needed for changing in phase of the workpiece controls laser drilling. In laser drilling, the incident beam energy has a spatial intensity distribution that is typically created by a laser working. Due to various heat loss effects, the mean diameter of the hole may be smaller than the diameter of the beam. The laser beam's diameter is depicted in figure (1) as well. These heat losses, which take the beam energy not fitting with actual position of hole drilling process, are principally caused by conduction into the interior of the metal drilled and consider losses to the surrounding.

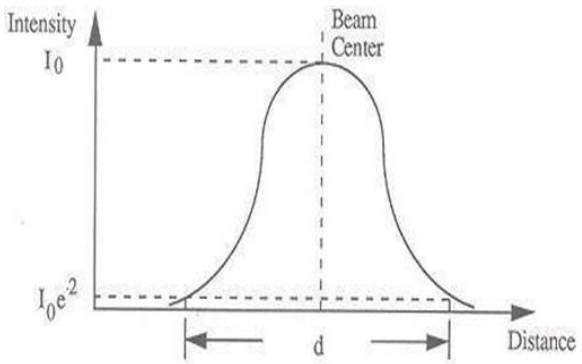

Figure 1. Distribution of intensity for laser beam [1]

Several physical phenomena during laser machining result in energy losses: If melting is a part of the material removal operation, reducing the laser beam's efficiency in two ways. The molten substance that has gathered in the hole may first be heated above its melting point using energy. Another source of heat loss in percussion drilling is the possibility of molten material resolidifying in between pulses. As a result, during each pulse, some of the beam energy is used to vaporized material. When materials like ceramics are evaporated, plasma production is possible. Above the beam-material interaction zone. A portion of the energy from the incoming laser beam is absorbed by this cloud, which raises its temperature until plasma is produced. But occasionally, the heated plasma serves as a second heat source, which enhances the drilling operation. Because it is challenging to manage the plasma's directionality, dimensional accuracy can be impacted. By removing vaporized material from the laser beam's path, the use of an inert assist gas can aid in decreasing the influence of plasma production. The spectrum absorptivity properties of the material being processed and the laser radiation's wavelength both affect how much of the laser beam energy is absorbed. Aluminum and copper are two metals that reflect a lot of CO_2 laser light (10.6 m wavelength), hence Nd: YAG lasers work best the laser is superior. The absorptivity of metals and ceramics is affected by the existence of molten layers, and a surface's absorptivity is also influenced by its orientation in relation to the beam direction. It is demonstrated that for incident angles greater than 800, the maximum amount of beam energy can be absorbed. The beam energy that the workpiece does not absorb is reflected in the opposite direction of the entering energy. Multiple beam reflections along the hole wall may happen for deep holes, reducing the amount of beam energy available for material removal. Through convective heat transfer, the use of a gas jet during laser drilling can help to cool the erosion front. More beam energy is needed to keep the erosion front's melting or vaporization temperature constant as thermal dissipation increases [1]. However, dimensional control of the reaction process becomes challenging since chemical reactions have a propensity to spread out in all directions. A technique called "trepanning" can be used to create large diameter holes (diameters more than 1.3 mm), in which the beam is scanned on a circular trajectory to determine the final geometry. The machining speed for the trepanning process, a circular through cutting procedure, is determined by the beam's scanning velocity. As long as the melt surface temperature does not significantly exceed the melting point and the evaporation rate is low enough, melt removal is typically believed to predominate when an aiding gas is given to the melt surface. Without an aiding gas present, melt expulsion varies with recoil pressure, which is largely influenced by surface temperature. Early simulations revealed that the phase change from the heat interaction zone removed a sizeable percentage of the laser power that was absorbed [1]. In-depth investigation has been made to create a theoretical framework for predicting the laser drilling response. Von Allmen used a one-dimensional transient gas dynamic model to investigate the drilling velocity and drilling efficiency under the assumption of a constant laser beam intensity profile [2]. A one-dimensional steady state model was created by Chan and Mazumder [3] to account for liquid expulsion, but the drilling process is transitory and the one-dimensional assumption is inappropriate for holes with high aspect ratios. The concept was expanded by Kar and Mazumder [4] to two-dimensional instances without taking into account melt ejection. Armon et al. used the Crank-Nicholson approach to solve a one-dimensional metal drilling issue that they had developed using the enthalpy balancing method [5]. They also performed an experimental examination on CO_2 laser drilling of metal, and they used their theoretical model to assess the experimental findings [6]. Ganesh et al. [7], who used a two-dimensional transient generalized model and included conduction, convection, and phase change heat transfer during laser drilling, gave a more thorough study of melt expulsion. This model, however, is computationally intensive. To investigate the impact of solid conduction on the rate of material loss and phase transition at interfaces, Zhang and Faghri created an analytical model [8]. The impact of phase changes on heat transport is not taken into account in this model. A Knudsen layer was taken into account at the melt-vapor front in a two-dimensional transient model created by Zhang et al. [9] without taking the phase change impact into account. By assuming linear temperature profiles for solid, liquid, and vapor [10] and making the implicit assumption that phase change has no impact on temperature gradient, Pastras et al. were able to examine the material removal efficiency. Some existing models have taken the phase change impact into account. For instance, the steady-state model created by Semak and Matsunawa [1] and a subsequent version modified by Low et al. [11] to investigated the phase change effect with an aiding gas on laser drilling. Ng et al. created a laser drilling model that noticed into account the impact of employing oxygen as an aiding gas. The average melt thickness is calculated by dividing the melt's thermal diffusivity by the average propagation velocity, which is based on the assumption that the melt front propagates at an averaged velocity [12]. Assuming a negligible vaporization rate, Zeng et al. devised a two-dimensional analytical model for optical trepanning [13]. By averaging cross-sections, Collins and Gremaud created a straightforward one-dimensional model while ignoring the role played by the radial flow velocity component [14]. A hat-top-shaped intensity profile is assumed in all phase change models created in [1, 2, 12] and the most recent simulation by Semak and Miller [15]. The conclusion of the phase change is directly impacted by the assumption regarding the laser beam intensity profile [16–18]. The melt surface temperature might be believed to be constant using the hat-top profile, despite a rapid shift happening towards the melt's edge. If it is further assumed that there is no shear traction during the phase change, It is also possible to believe that the recoil pressure is constant, which overestimates the significance of melt expulsion. Therefore, a more accurate model should be used to reevaluate the phase change

effect on laser drilling. Based on the actual physics involved, a more accurate model should take vaporization into account. It is well known that vaporization happens whenever a substance is heated over its melting point and that the melt surface temperature has a significant impact on the recoil pressure. However, while other earlier models used the boiling point for the liquid-to-vapor transition [19], others assumed a Stefan condition at the melt-vapor interface [7]. Solana and others believed that the Gaussian shape of the recoil pressure [20]. According to Li et al. hypothesis's the liquid-to-vapor transition occurs over a specific temperature range [21]. It's crucial to more properly simulate heat conduction in order to forecast real physics. Heat conduction in solids is a classical problem, but since laser drilling entails a change in boundary conditions, different investigators have taken diverse approaches to the issue. A steady state heat conduction model was studied on the basis of constant melting layer thickness [22]. By assuming that the phase transition from solid to vapor takes place in a single step, Modest investigated a transient heat conduction model [23]. The partial differential equation was solved by explicit scheme to find out temperature profile; Zhang and Faghri then used this equation to arrive at an integral solution [8]. By assuming an exponential temperature profile, Shen et al. also developed a model of transient heat conduction [24]. Ho and Lu created a transient heat conduction model by using a solid heat source term to symbolize the laser beam's energy flux [25]. By assuming that the substance being heated is initially at its melting point, Shidfar et al. constructed a transient heat conduction model [26]. These models have all had certain limitations as a result of the assumptions made, but they have all been frequently cited in the laser simulation research field and helpful in understanding the physics to varying degrees. Because laser drilling in a solid uses thermal energy from laser beams, which is a transient heat conduction process, classical approaches [27] can be used to create a theoretical model that could more accurately anticipate the process while making fewer assumptions. That is effort, creating a theoretical model that specifically accounts for the phase change impact. The phase change effect on heat transfer can be confidently assessed after the solution on the phase change velocity is made accessible. To save on computational costs, keep the model as simple as you can. In contrast to earlier research. The vapor temperature and the first melting time all fluctuate radially when the laser beam is considered to have a Gaussian intensity profile. The solid's absorption of heat and its transmission by Both phase change and phase change are considered. The momentum equation and the energy equation are derived using both the boundary layer formulation and integral forms. Finally, using the suggested methodology, a series of numerical tests are carried out on a unique super alloy. The deep q-learning method, which is a member of the reinforcement learning type, is one of the often-used machine learning techniques to control physical equipment [28]. Instead of requiring positive or negative labels, it enables a robot to discover the greatest placement accuracy through trial-and-error interactions with the environment [29]. It gradually identifies the optimal robotic operation as part of the general robotic operation optimization discovers the greatest cumulative payoff value using the optimum placing technique in each iteration. Using the deep q-learning method in the context of industrial robots has two key benefits: it allows for the incorporation of collected live video data [30,31] and the avoidance of well-known machine learning issues like overfitting. Deep q-guiding learning's idea is built on how a robot perceives its environment [32], assesses its current condition, and takes appropriate action to maximize reward. Previous studies shown the applicability of this technique for defining the robot tool position by Using visual information, determining the ideal configuration of robot motion parameters, and producing output results with corrected set point coordinates [33] are all important. Since online robot training takes a lot of time, positioning accuracy metrics can be calculated using machine learning simulation for real-world scenarios. Physical experiments that take more than five hours are replaced by simulations that last less than five minutes. The simulation is practical in that it simply needs a computer (except when it is necessary to collect input data from there al robotic system). However, due to the assumptions and oversimplifications employed to explain various variables, no simulation can accurately reflect the actual world. unidentified or unclear bodily effects. Therefore, even if the technique is effective, simulation findings still need to be verified by experiments carried out under real-world circumstances. As a result, choosing the most promising sets of algorithm parameter combinations for testing in the actual world using simulation is a great strategy. By contrasting simulations and utilizing the articulated robot as a workbench, the methodology was assessed. A computational methodology was developed to simulate the phase change processes and a thermal model was simulated to determine the spatial and temporal temperature profile of the phase change location [40].

2. Interface Energy Balance

The coordinate system used to formulate the equations has an origin at the solid-vapor boundary, with (r) standing for radial orientation and (z) for downward direction pointing to evaporate from the solid. The shift in the interface between phases is denoted by the lowercase letter (z).

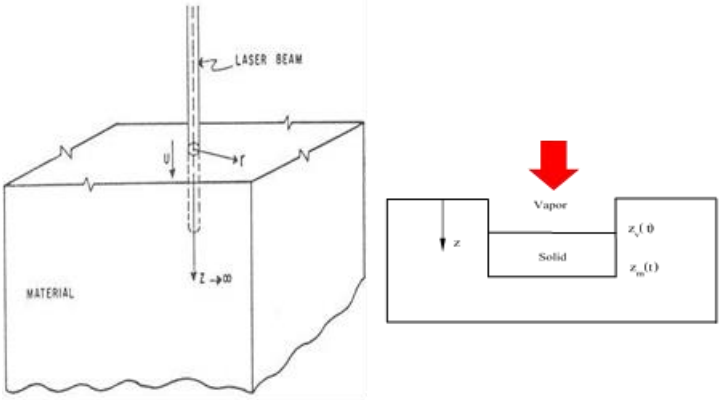

Figure 2. Laser drilling physical model and systems coordinate.

Table 1. Thermophysical characteristics of steel material

Melting latent heat	L_{ls}	2.26×10^{4} (J kg^{-1})
Vaporization latent heat	L_{lv}	7.12×10^{6} (J kg^{-1})
Melt density	ρ	7.8×10^{3} (kgm^{-3})
Molar mass of vapor	M	0.069 (kg mol^{-1})
Initial temperature	T_i	297.15 K
Melting temperature	T_m	1540˚C
Saturation temperature	T_{sat0}	3140˚C
Saturation pressure	p_0	1.01325×10^{5} (Nm^{-2})
Liquid thermal conductivity	k_l	20.90 (Wm^{-1} K^{-1})
Vapor thermal conductivity	k_v	0.034 (Wm^{-1} K^{-1})
Solid thermal conductivity	k_s	50.2 (Wm^{-1} K^{-1})
Liquid specific heat	cp_l	615 (J kg^{-1} K^{-1})
Solid specific heat	cp_s	372 (J kg^{-1} K^{-1})
Radius of laser beam	R	0.25×10^{-3} (m)

2.1 Melt convection

The governing equations in the layer of melt. The continuity, momentum and energy equation can be expressed as follows, which is similar to the presumptions in the jet impingement study by Kendoush [34].

$$\frac{\partial u}{\partial r}+\frac{\partial v}{\partial z}+\frac{u}{r}=0 \tag{1}$$

$$u\frac{\partial u}{\partial r}+v\frac{\partial u}{\partial z}=\frac{\mu}{\rho}\left[\frac{\partial^2 u}{\partial z^2}+\frac{1}{r}\frac{\partial u}{\partial r}-\frac{u}{r^2}\right]-\frac{1}{\rho}\frac{\partial p}{\partial r} \tag{2}$$

$$\frac{\partial T_l}{\partial t}+u\frac{\partial T_l}{\partial r}+v\frac{\partial T_l}{\partial z}=\alpha_l\frac{\partial^2 T_l}{\partial z^2} \tag{3}$$

where the radial and vertical velocity components, respectively, are denoted by u and v. Both the melt's density and viscosity are represented.

$$-\frac{1}{\rho}\frac{\partial p}{\partial r}=U\frac{dU}{dr} \tag{4}$$

By assume that the pressure fluctuation in the thickness direction is ignorable because the melt layer is significantly thinner than its lateral dimension. As a result, the second momentum conservation equation becomes and pressure can only be thought of as a function of radius.

2.2 Energy balance at solid- Vapor interface

The vapor provides the energy for both evaporating and heating the solid, hence the energy balance at the solid-vapor contact can be expressed as follows,[40]:

$$\rho L V_{s2} = k_s \frac{\partial T_s}{\partial z} - k_v \frac{\partial T_v}{\partial z} \quad (5)$$

where k_s and k_v stand for the solid and vapor thermal conductivity, respectively, and L stands for the latent heat of evaporation. The density of the solid is considered to be the same as the fluid's density in this equation.

2.3 Heat conduction in solid

The solid surface gets constant heat flow before the surface temperature reaches the vaporization threshold, and when the boundary condition is imposed, r=0,z=0, the solution of the heat equation becomes,[41]

$$\frac{1}{\alpha_s}\frac{\partial T_s}{\partial t} = \frac{\partial^2 T_s}{\partial r^2} + \frac{1}{r}\frac{\partial T_s}{\partial r} + \frac{\partial^2 T_s}{\partial z^2} + \frac{Q}{k} \quad (6)$$

Where is the absorption energy $Q = (1-R)I_{\circ}\exp\left[(-\delta z)(\frac{r^2}{z^2}\right)$ and $I_{\circ}$ is laser intensity ,R is the reflectivity, δ is distance from the surface

By applying the finite difference method with explicit scheme the heat equation will be become:

$$T_{i,j}^{n+1} = 4\lambda T_{i+1,j}^{n} + (1-6\lambda)T_{i,j}^{n} + 2\lambda T_{i,j+1}^{n} + \frac{Q\alpha\Delta t}{k} \quad (7)$$

At r>0.z=0 the heat equation become

$$T_{i,j}^{n+1} = (\lambda + \frac{\alpha\Delta t}{2r\Delta r})T_{i+1,j}^{n} + (1-4\lambda)T_{i,j}^{n} + (\boldsymbol{\lambda} - \frac{\alpha\Delta t}{2r\Delta r})T_{i-1,j}^{n} + 2\boldsymbol{\lambda} T_{i,j+1}^{n} + \frac{Q\alpha\Delta t}{k} \quad (8)$$

When r>0.z>0 the heat equation become

$$T_{i,j}^{n+1} = (\lambda + \frac{\alpha\Delta t}{2r\Delta r})T_{i+1,j}^{n} + (1-4\lambda)T_{i,j}^{n} + (\boldsymbol{\lambda} - \frac{\alpha\Delta t}{2r\Delta r})T_{i,j}^{n} + \boldsymbol{\lambda} T_{i,j+1}^{n} + \boldsymbol{\lambda} T_{i,j-1}^{n} + \frac{Q\alpha\Delta t}{k} \quad (9)$$

where is the dimensionless temperature within the solid, whereas Ts stands for the dimensional value; is the solid's starting dimensionless temperature; Ti stands for the dimensional value; and Tv is the evaporation point, also known as the similarity variable. In this investigation, both the geometrical adjustment for the temperature gradient and the precise answer for the time after melting begins were obtained. It consists of three parts,

2.4 Heat conduction in interface

Conduction of energy was the heat transfer process at the interface as the phase changed from solid to vapor.. At r=0.z0, the boundary conditions will be applied.

$$T_{i,j}^{n+1} = 4\lambda T_{i+1,j}^{n} + (1-6\lambda)T_{i,j+1}^{n} - \frac{2\lambda\rho_s L_s v\Delta z}{k} + \frac{Q\alpha\Delta t}{k} \quad (10)$$

2.5 Heat conduction in Vapor Phase

The same suggested mathematical model was used to calculate the temperature distribution in the vapor phase. Calculating the value of vapor's velocity and temperature at each position requires adding the vapor's velocity to the energy equation's component parts. Boundary condition application at r=0,z=0.

$$\frac{1}{\alpha_v}\frac{\partial T_v}{\partial t} + \frac{u_z}{\alpha_v}\frac{\partial T_v}{\partial z} = \frac{\partial^2 T_v}{\partial r^2} + \frac{1}{r}\frac{\partial T_v}{\partial r} + \frac{\partial^2 T_v}{\partial z^2} + \frac{Q}{k} \quad (11)$$

$$T_{i,j}^{n+1} = 4\lambda T_{i+1,j}^{n} + (1-6\lambda)T_{i,j}^{n} + \left(\lambda - \frac{u_z\Delta t}{2\Delta z}\right)T_{i,j+1}^{n} + \left(\lambda + \frac{u_z\Delta t}{2\Delta z}\right)T_{i,j-1}^{n} + \frac{Q\alpha\Delta t}{k} \quad (12)$$

When the domain of r-z plane at r> 0,z>0 then heat equation become as follows:

$$T_{i,j}^{n+1} = \left(\lambda + \frac{\alpha_v\Delta t}{2r\Delta r}\right)T_{i+1,j}^{n} + (1-4\lambda)T_{i,j}^{n} + \left(\lambda - \frac{\alpha_v\Delta t}{2r\Delta r}\right)T_{i,j+1}^{n} + \left(\lambda - \frac{u_z\Delta t}{2\Delta z}\right)T_{i,j+1}^{n} + \left(\lambda + \frac{u_z\Delta t}{2\Delta z}\right)T_{i,j-1}^{n} + \frac{Q\alpha\Delta t}{k} \quad (13)$$

3. Deep Learning Method

The robot was operated by a special software platform made up of six combined parts. All software modules, which are primarily developed in the Python language, run concurrently and carry out separate tasks. The robot operating system, extra drivers, and libraries are used to communicate with external devices. The latter uses specialized drivers and libraries supplied by the manufacturer to communicate with the robot. The deep learning algorithm is part of the machine learning control module that was constructed. The global module, which synchronizes global variable values across several Python programs executing on the control system, provides it with the values of global variables. The control module for machine learning interacts with the main system, accepting input values and sending the results of the machine learning algorithm. The data input/output routines and simulation methods are also included in the main module. The command is sent from the main to the vision module, which uses a digital microscope to take a snapshot of the target, identify it, determine its center coordinates, and send those coordinates back to the main.

3.1. Implementation of the Method

The simulation algorithm operating in the Main module is a cycle carrying out certain tasks repeated repeatedly over a large number of iterations (300–5000). Five values from the previous cycle are entered to start the cycle. The parameter's value is 0 when the cycle is first executed. In the other situations, the algorithm uses the preceding cycle's correction step and the r and z direction deviation values. The output of machine learning is a single natural number, which is then converted to the proper corrective steps to be stored in the memory. The corrective step is an iterative adjustment that takes the shape of a vector. An array is used here first. contains all of the defined vectors is produced. Next, it is presumed that the machine learning output that is accepted is an index of that array. Each output value has the relevant adjustment step applied to it. To acquire the corrected coordinates, the vector component of the correction step is redefined using the target's spatial coordinates. The algorithm's objective is to get coordinates that have been rectified. The corrective steps build upon one another. They keep adding the outcomes of the most recent iteration to the outcomes of all earlier iterations. The robot is given the order to execute the revised coordinates in real time after defining them. The vision module calculates the real target coordinates, captures the target image, and transmits a message instructing the robot to go back to its "home" position. To ascertain the values and orientations of the deviations, the theoretical and actual target coordinates are compared. The primary module can also carry out tasks for ease and speed. simulations that use or don't use real data that has been gathered. The majority of the Main code's blocks are used in the simulation. The distinction is that the simulation makes use of data gathered while the robot was moving thousands of times without correction rather than giving directions to the robot and camera. These numbers reflect the robot's actual positioning accuracy. It is possible to use such a dataset in an infinite number of simulations. Additionally, by filling the algorithm memory with actual data before beginning the online training, it reduces the necessary number of iterations.

4. Results and discussion

Conduction-flow instances should first be simulated, then the case of pure conduction. Table 1 is a list of the thermo-physical characteristics employed. In the numerical modeling, we investigated the range from 2.51010W m^{-2} to 16.01010W m^{-2} where the laser intensity at the center varies from 5.31010W m^{-2} to 14.31010W m^{-2}. Similar to Zhang and Faghri [8], the effect of the target material's absorptivity was disregarded in this work. The current model incorporates the same laser pulse duration and beam intensity profile as those provided by Zhang and Faghri [8]. the simulation's time step was. The hole appeared to develop much more quickly in the drill direction than in the lateral direction. These profiles resemble one another as well as the ones Zhang and Faghri predicted [8]. The thickest melt layer is found close to the boundary of the melt zone, when the vaporization begins to become undetectable, and it is seen that the thickness of the melt layer grows in a radial direction. Additionally, it has been noted that the rate of vertical drilling is nearly constant. With increased laser beam intensity in the plan, the temperature distribution in the solid phase rose.(r-z) plane of effective as shown in figure 3. The temperature values represent the variation of conduction heat transfer mechanism.

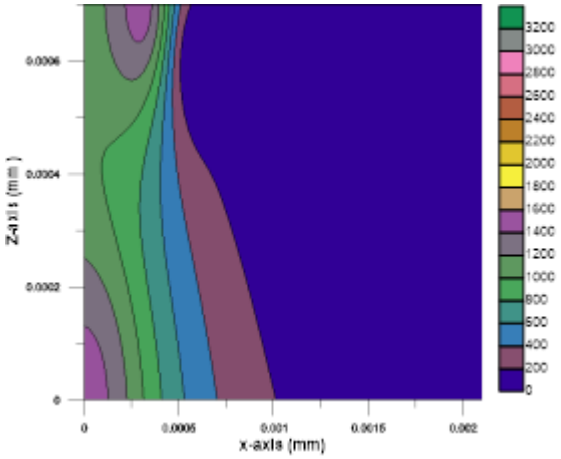

Figure 3. Contour of temperature distribution through solid phase in the (r-z) plane at 3ms

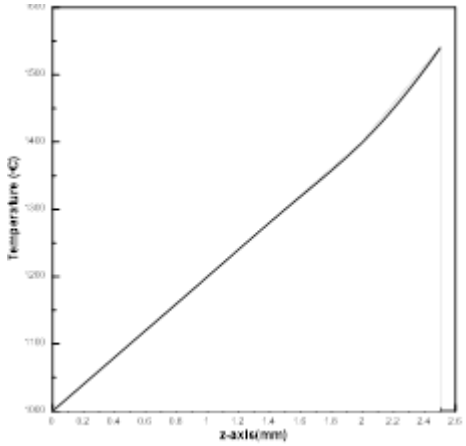

Figure 4. Temperature distribution through solid phase at 3ms

The temperature at the summit of the melt can be predicted using the mathematical model. Figure 4 shows that the vapor recoil pressure increases with increasing laser beam intensity. The pressure within the melt zone resembles Gaussian curves rather than being uniform. As the laser intensity raises, it is seen that the temperature rises. At the vapor zone's edge, it had a sharp slope. Additionally, the modeling outcomes revealed that the temperature and With the exception of a sudden rise at the beginning, pressure is mostly steady during a laser beam impulse. Figures 5. and 6. demonstrate how rising profile models and rising-fall profile models both confirm this pattern. The rising models indicate the interface line is started and the phase transition is occurring, and it is projected that the peak flow velocity will first experience a quick drop before reaching a fairly steady stage later. It differs little from what was anticipated by rising-fall models with parameter. Numerous variables affect how the phase change affects material removal. The Prattle number is one element. the velocity of the vertical phase change and the rate of vaporization as anticipated by a parameter model. One location—close to the center of the laser beam—is where the phase change takes place. It was seen that as the vaporization rate increased, the melting rate rapidly decreased and quickly found equilibrium. The phase change velocity was far lower than the vaporization rate, by a factor of around 2.5. Results from other profile models were comparable. Using a completely different methodology, a recent study revealed that natural convection does not significantly affect melt transport and melting pool geometry [36]. However, if the substance has different properties, the phase change might have a varied effect on how much material is removed. To demonstrate this argument, a test was done with the same additional parameters as the numerical test. Phase change has been noticed. The free flow zone was absent from the majority of the melt zone. The fact that the beam center was determined using a pure operational model conduction-flow that caused the solid-vapor interface to shift differently. When a particle has more energy, it will be transported to a higher level, where its phase will change to vapor. The border condition is arguably the most contentious topic. The second node makes a very approximate approximation of it because it is unavailable at the beam center. Nevertheless, we continued to attempt to assess the phase change using.

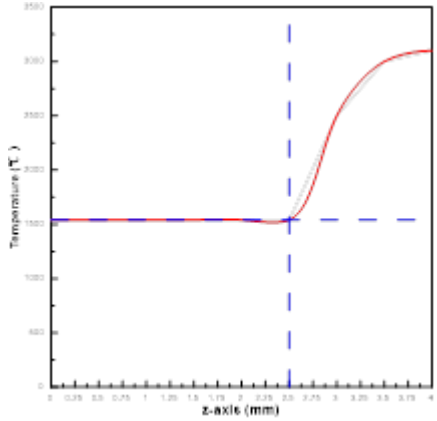

Figure 5. Temperature distribution through interface at time 4 ms

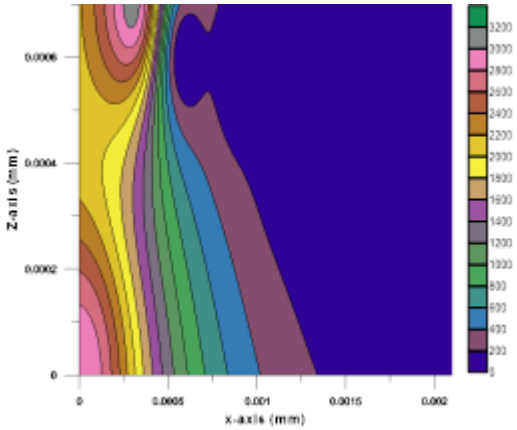

Figure 6. Contour of temperature distribution through interface in the (r-z)plane at 4 ms

The vapor phase started after the phase change phenomenon occurs at the time 4 ms when the temperature value 1620 ^{o}C as shown in figure(7and 8). A mathematical model was evaluated the direct simulation of time-dependent phase process is solving the evaporation processes, and the temperatures distribution through laser drilling process. This depending upon many assumptions for each phase and the moving boundary condition inside domain (interface). Thermo-physical properties of each phase remain uniform and constant,[41]

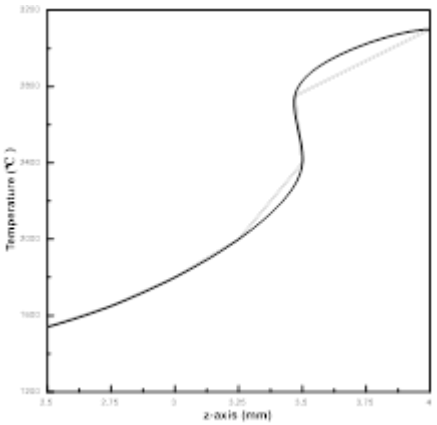

Figure7. Temperature distribution through z-axis in vapor phase. At 6ms

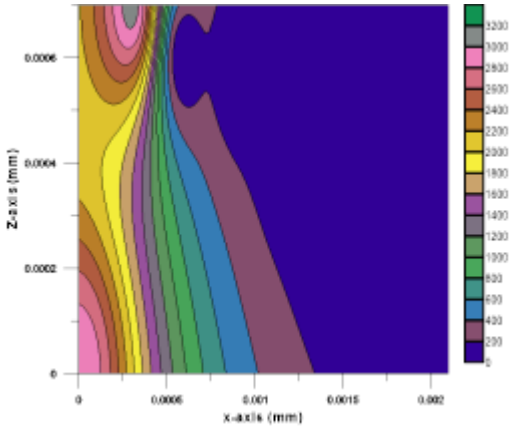

Figure 8. Contour of temperature distribution through vapor phase in the (r-z) plane at 6 ms

In contrast to the uncorrected situation, the dependencies of the corrected position with respect to iteration, as shown in figure 9, reveal significant differences in position coordinates in the learning positionafter about 230 iterations. Because the algorithm does exploration at the beginning of the training, this behavior is highly anticipated. At the conclusion of this phase, the accuracy characteristics underwent asignificant modification, and these coordinate values became significantly high stable. The amplitudeof fluctuations in the vertical axis is greater than in the radial axis, much like in the case of uncorrected moving. The process perspective is much more steady with the updated location, and both coordinates remain unchanged. essentially constant .Figure 10 explains how the absolute inaccuracy in terms of the number of iterations needed to calculate the robot's explain the positioning accuracy varies over time. With more iterations, as was predicted, the positional deviation grows, and in the short run, there are noticeable swings in the random error value.

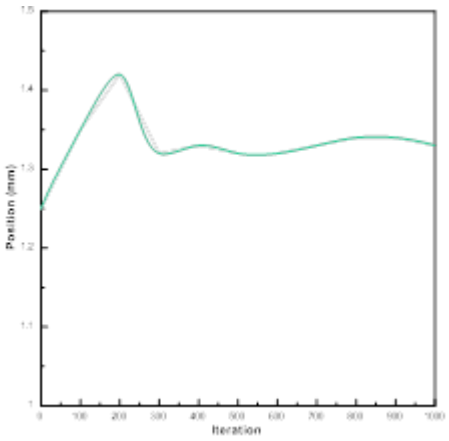

Figure 9. Variation of position for final coordinates of r-axis

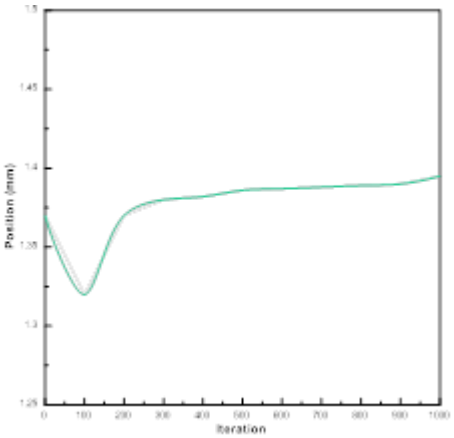

Figure10. Variation of position for final coordinates of z-axis

The position deviation graph provides a clear illustration of how the machine learning result differs from the initial condition. Here, it is evident that the error value remains roughly constant and is equal to that which occurs at the start of the uncorrected positioning after the transient learning phase ends and the steady learning phase starts. In spite of the fact that the mean error value still resembles the value that first appears at the start of the uncorrected positioning, this condition shows that the algorithm is successful in eliminating positioning drift.. The algorithm parameters discovered from the simulations were used to assess the accuracy of the robot positioning. Figure 11 illustrates how the position of the robot end effector changes over the course of 800 motion cycles based on the dependency of relative position with respect to iterations. The positional deviation exhibits nearly identical amplitudes and trends in the r and z axes, measuring 0.08 mm in the z axis (from 1.10 to 1.18 mm) and 0.07 mm in the r axis (from1.08mm to 1.15mm). This discrepancy may be explained by the fact that the robot's mobility is mostly affected in the vertical direction by the load it is carrying.

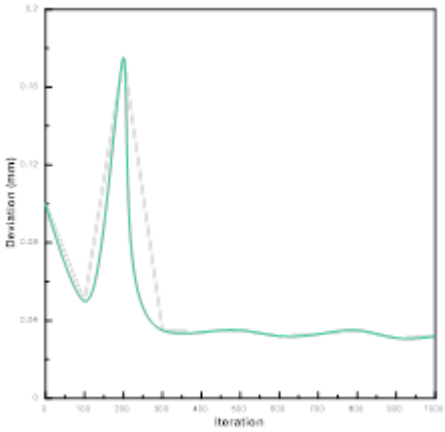

Figure 11. Variation of position error with No. of iterations

5. Conclusions

. According to the investigations, the momentum conservation equation explicitly includes the phase change effect on laser drilling. The solution of the phase transition is found by applying the moving boundary condition in the solid-vapor interface with happening of phase change phenomenon and utilizing the explicit approach for solving the energy equation. Additionally, the temperature field's integral solution is discovered. Additionally, the precise remedy for heat conduction is created. The exact answer to the Stefan problem's solution is made up primarily of this solution, so it can also be utilized as a rough solution to increase computational efficiency. The suggested model is more accurate to the actual mechanics at play than earlier ones. utilizing a super alloy with the new model. A precise solution for heat conduction is also developed. The Stefan problem solution can be used as a rough solution to increase computer efficiency because it is a crucial component of the precise answer. Using machine learning techniques, it is possible to demonstrate the dependence of the saturation temperature on the robot positioning accuracy. The robot location inaccuracy was reduced from 0.07 mm to 0.02 mm by the deep learning system, demonstrating its effectiveness. This outcome emerged after the training process had gone through about 800 iterations. the just made technique shortens the time required for the machine learning process while increasing the precision and reliability of robot positioning. A unique neural network is used in the developed methodology for simulation with numerous input parameters. Without having access to the internal robot control system, the external compensation for the robot's positional drift in the target point proved effective.

Nomenclature

c_{pl}, specific heat of the liquid (J kg^{-1} K^{-1})

c_{ps}, specific heat of the solid [J kg^{-1} K^{-1})

L_s latent heat of solid (J kg^{-1}),

L_v latent heat of vaporization (J kg^{-1})

I_0, laser intensity at the center (W m^{-2})

j_v, Vaporization molar flux (kg s^{-1})

k_l Liquid thermalconductivity (Wm^{-1} K^{-1})

k_s, Solid thermalconductivity (Wm^{-1} K^{-1})

M, Gas molarmass (kg mol^{-1})

T_i, Solid initialtemperature (K)

T_m, Solid liquidinterface meltingtemperature (K)

T_{sat0}, Saturationtemperature at pressure p_0, (K)

T_{sat}, saturationtemperature at pressure p, (K)

t_p, pulseon time, (s)

U, dimensionless radial velocity of free flow

V, dimensionless vertical velocity of free flow

V_v, Vapor velocity at th melt surface

u, Tangentialvelocity (m s^{-1})

v, normalvelocity (m s^{-1})

α_l, Meltthermal diffusivity , $\frac{k_l}{\rho c_{pl}}$

References

[1] V. Semak, A. Matsunawa, The role of recoil pressure in energy balance during laser materials processing, Journal of Physics D: Applied Physics, 30(18) (1997) 2541-2552.

[2] M.V. Allmen, Laser drilling velocity in metals, J. Applied Physics, 47 (1976) 5460-5463.

[3] C.L. Chan, J. Mazumder, One-dimensional steady-state model for damage by vaporization and liquid expulsion due to laser-material interaction, J. Applied Physics, 62(11) (1987) 4579-4586.

[4] A. Kar, J. Mazumder, Two-dimensional model for material damage due to melting and vaporization during laser irradiation, J. Applied Physics, 68(8) (1990) 3884-3891.

[5] E. Armon, Y. Zvirin, G. Laufer, A. Solan, Metal drilling with a CO_2 laser beam. I. Theory, J. Applied Physics, 65(12) (1989) 4995-5002.

[6] E. Armon, M. Hill, I.J. Spalding, Y. Zvirin, Metal drilling with a CO2 laser beam. II. Analysis of aluminum drilling experiments, J. Applied Physics, 65(12) (1989) 5003-5006.

[7] R.K. Ganesh, A. Faghri, Y. Hahn, A generalized thermal modeling for laser drilling process - I. Mathematical modeling and numerical methodology, Int. J. Heat Mass Transfer, 40(14) (1997) 3351-3360.

[8] Y. Zhang, A. Faghri, Vaporization, melting and heat conduction in the laser drilling process, Int. J. Heat Mass Transfer, 42(10) (1999) 1775-1790.

[9] W. Zhang, Y.L. Yao, K. Chen, Modelling and analysis of UV laser micromachining of copper, Int. J. Adv. Manuf. Technol. , 18(5) (2001) 323-331.

[10] G. Pastras, A. Fysikopoulos, P. Stavropoulos, G. Chryssolouris, An approach to modelling evaporation pulsed laser drilling and its energy efficiency, International Journal of Advanced Manufacturing Technology, 72(9-12) (2014) 1227-1241.

[11] D.K.Y. Low, L. Li, P.J. Byrd, Hydrodynamic physical modeling of laser drilling, Journal of Manufacturing Science and Engineering, Transactions of the ASME, 124(4) (2002) 852862.

[12] G.K.L. Ng, P.L. Crouse, L. Li, An analytical model for laser drilling incorporating effects of exothermic reaction, pulse width and hole geometry, International Journal of Heat and Mass Transfer, 49(7-8) (2006) 1358-1374.

[13] D. Zeng, W.P. Latham, A. Kar, Two-dimensional model for melting and vaporization during optical trepanning, Journal of Applied Physics, 97(10) (2005).

[14] J. Collins, P. Gremaud, A simple model for laser drilling, Mathematics and Computers in Simulation, 81(8) (2011) 1541-1552.

[15] V.V. Semak, T.F. Miller, Simulation of laser penetration efficiency, Journal of Physics D: Applied Physics, 46(38) (2013).

[16] L. Han, F.W. Liou, Numerical investigation of the influence of laser beam mode on melt pool, International Journal of Heat and Mass Transfer, 47(19-20) (2004) 4385-4402.

[17] S.Z. Shuja, B.S. Yilbas, Laser produced melt pool: Influence of laser intensity parameter on flow field in melt pool, Optics and Laser Technology, 43(4) (2011) 767-775.

[18] O. Momin, S.Z. Shuja, B.S. Yilbas, Laser heating of titanium and steel: Phase change at the surface, International Journal of Thermal Sciences, 54 (2012) 230-241.

[19] Y. Zhang, Z. Shen, X. Ni, Modeling and simulation on long pulse laser drilling processing, International Journal of Heat and Mass Transfer, 73 (2014) 429-437.
[20] P. Solana, P. Kapadia, J. Dowden, W.S.O. Rodden, S.S. Kudesia, D.P. Hand, J.D.C. Jones, Time dependent ablation and liquid ejection processes during the laser drilling of metals, Optics Communications, 191(1-2) (2001) 97-112.
[21] J.F. Li, L. Li, F.H. Stott, A three-dimensional numerical model for a convection-diffusion phase change process during laser melting of ceramic materials, International Journal of Heat and Mass Transfer, 47(25) (2004) 5523-5539.
[22] C.L. Chan, J. Mazumder, One-dimensional steady-state model for damage by vaporization and liquid expulsion due to laser-material interaction, Journal of Applied Physics, 62(11) (1987) 4579-4586.
[23] M.F. Modest, Three-dimensional, transient model for laser machining of ablating/decomposing materials, International Journal of Heat and Mass Transfer, 39(2) (1996) 221-234.
[24] Z.H. Shen, S.Y. Zhang, J. Lu, X.W. Ni, Mathematical modeling of laser induced heating and melting in solids, Optics and Laser Technology, 33(8) (2001) 533-537.
[25] C.Y. Ho, J.K. Lu, A closed form solution for laser drilling of silicon nitride and alumina ceramics, Journal of Materials Processing Technology, 140(1-3 SPEC.) (2003) 260-263.
[26] A. Shidfar, M. Alinejadmofrad, M. Garshasbi, A numerical procedure for estimation of the melt depth in laser material processing, Optics and Laser Technology, 41(3) (2009) 280284.
[27] W. Rohsenow, J. Hartnett, Y. Cho, Handbook of Heat Transfer, 3 ed., McGraw-Hill Education, New York, 1998.
[28] Ribeiro, T.; Gonçalves, F.; Garcia, I.; Lopes, G.; Ribeiro, A.F. Q-Learning for Autonomous Mobile Robot Obstacle Avoidance. In Proceedings of the 19th IEEE International Conference on Autonomous Robot Systems and Competitions (ICARSC) 2019, Porto, Portugal, 24–26 April 2019.
[29] Koushik, A.M.; Hu, F.; Kumar, S. Deep q-learning-based node positioning for throughput-optimal communications in dynamic UAV swarm network. IEEE Trans. Cogn. Commun. Netw. 2019, 5, 554–566.
[30] Gankidi, P.R.; Thangavelautham, J. FPGA architecture for deep learning and its application to planetary robotics. In Proceedings of the IEEE Aerospace Conference Proceedings, Big Sky, MT, USA, 4–11 March 2017; IEEE Computer Society: Washington, DC, USA, 2017.
[31] Edu, J.; Wang, Z.; Xie, Y.; Yang, Z.; Bayen, A.; Jadbabaie, A.; Pappas, G.J.; Parrilo, P.; Recht, B.; Tomlin, C.; et al. A Theoretical Analysis of Deep Q-Learning Jianqing Fan. PMLR 2020, 120, 486–489.
[32] Gordón, C.; Encalada, P.; Lema, H.; León, D.; Castro, C.; Chicaiza, D. Intelligent Autonomous Navigation of Robot Kuka Youbot. Advances in Intelligent Systems and Computing; Springer: Berlin, Germany, 2020; Volume 1038, pp. 954–967.
[33] Rahman,M.M.;Rashid,S.M.H.;Hossain,M.M.ImplementationofQlearninganddeepQnetworkforcontrollingaselfbalancing robot model. Robot. Biomim. 2018, 5, 8. [CrossRef]
[34] A.A. Kendoush, Theory of stagnation region heat and mass transfer to fluid jets impinging normally on solid surfaces, Chem. Eng. Proc., 37(3) (1998) 223-228.
[35] R. Bellantone, R.K. Ganesh, Analytical model for laser hold drilling final report: Contract II, in: E.H. report submitted to Pratt and Whitney Aircraft, CT (Ed.), 1991.
[36] A. Faghri, Y. Zhang, J.R. Howell, Advanced Heat and Mass Transfer, Global Digital Press, Columbia, MO, 2010.
[37] D. Burden, R. Faires, Numerical Analysis, Thomson Brooks/Cole, 2012.
[38] S.P. Kar, P. Rath, A fixed-grid based mixture model for pulsed laser phase change process, Computational Thermal Sciences, 6(1) (2014) 13-26.
[39] L.C. Evans, Partial Differential Equations, in, American Mathematics Society, 1997, pp. 662.
[40] AbdAli J, Alwan A , Theoretical Model to Investigate the Heat Transfer Mechanism through a Heat Pipe with Graphene Oxide/Distilled Water as Working Fluid,2020 IOP Conf. Series: Materials Science and Engineering 987 012017.
[41] Jihad Kadhim AbdAli,Maysoon Khazaal Abbas Maaroof, Modeling and Analysis of Thermal Pipe by Mathlab to Greenhouse Heating ,Eurasian Journal of Engineering and Technology, Volume 9 | August, 2022